Macromolecules

pubs.acs.org/Macromolecules Article

Effect of Added Salt on Disordered Poly(ethylene oxide)-*Block*-Poly(methyl methacrylate) Copolymer Electrolytes

Neel J. Shah, Sajjad Dadashi-Silab, Michael D. Galluzzo, Saheli Chakraborty, Whitney S. Loo, Krzysztof Matyjaszewski, and Nitash P. Balsara*

Cite This: *Macromolecules* 2021, 54, 1414−1424 Read Online

ACCESS | Metrics & More | Article Recommendations | Supporting Information

ABSTRACT: We studied the effect of salt addition on a diblock copolymer system with a negative Flory−Huggins interaction parameter, χ, indicative of attractive interactions between the two blocks. The system studied is poly(ethylene oxide)-*block*-poly(methyl methacrylate) (PEO-PMMA) with added lithium bis(trifluoromethanesulfonyl)imide (LiTFSI) salt. We studied two asymmetric block copolymers, PEO-PMMA(10−33) and PEO-PMMA(10−64), where the numbers refer to the molar masses of the blocks in kg mol^{-1}. The small-angle X-ray scattering (SAXS) profiles for PEO-PMMA(10−33) were featureless at all salt concentrations. In contrast, PEO-PMMA(10−64) exhibited SAXS peaks when the salt concentration was between $0.22 \leq m$ (mol Li/kg polymer) ≤ 0.44. The appearance of SAXS peaks only in PEO-PMMA(10−64) is consistent with the predictions of ionic self-consistent field theory developed by de la Cruz and co-workers, which predicts that in systems with negative χ, ordered phases are only found when the volume fraction of the ionic block is about 10%.

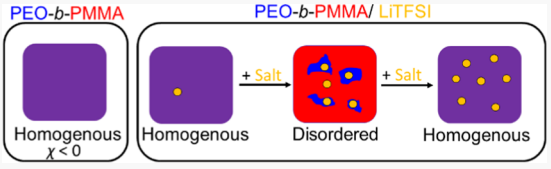

INTRODUCTION

There is continuing interest in the thermodynamic driving forces that underlie the transition from disorder to order in block copolymers.[1−7] At sufficiently high temperatures, entropy dominates and block copolymers are disordered. In the simplest of systems, lowering temperature results in the formation of periodic ordered structures that depend mainly on the composition of the copolymers. The disorder-to-order phase transition is governed by three parameters: the Flory−Huggins interaction parameter, χ, overall chain length, N, and the volume fraction of one of the blocks, ϕ. The phase diagram of block copolymer melts is usually shown on a χN versus ϕ plot.[1−4,8−10] An example of such a plot is shown in Figure 1a where we plot the results of the self-consistent field theory (SCFT) obtained by Cochran and Fredrickson.[3] This well-established phase diagram is symmetric about $\phi = 0.50$; implying for a given chemistry, the chain length at which ordering is seen is lowest for symmetric block copolymers with $\phi = 0.50$. In other words, in systems with a small enough χ parameter such that the disordered phase can be accessed, the driving force for order formation at constant N is largest at $\phi = 0.50$.

The effect of added salt on block copolymer thermodynamics has attracted considerable attention in recent years.[11−23] The extent to which the classical block copolymer phase diagram applies to salt-containing block copolymers remains an interesting open question. It has long been recognized that many observations on the phase behavior of block copolymers wherein the salt interacts strongly with one of the blocks can be rationalized by defining an effective χ parameter, χ_{eff}, that reflects interactions between the two blocks in the presence of salt. The concept of Born solvation introduced by Wang and co-workers provided a rational basis for the use of χ_{eff}.[24] Significant progress was made by determining χ_{eff} empirically and mapping the observed phase behavior on the classical block copolymer phase diagram for uncharged blocks.[25,26] In an important paper, de la Cruz and co-workers[18] introduced an approach that they called the ionic self-consistent field theory to predict the phase behavior of charged block copolymers. This theory was originally developed for the case when one of the block copolymers contained charged monomers, but more recent work by Qin and co-workers shows that similar phase behavior is obtained when salt was added to a neutral diblock copolymer.[20] We show one of the phase diagrams taken from ref 18 in Figure 1a (Figure 4c of ref 18).[18] The striking difference in the phase behavior between pure block copolymers and those with added salt is the appearance of a narrow chimney in the vicinity of $\phi = 0.10$, where ϕ is the volume fraction of the block with a high affinity for the salt ions such as poly(ethylene oxide) (PEO). It should be noted that the ionic SCFT phase diagram is plotted assuming that the ions are solvated exclusively in the PEO block; the model in ref 18 assumes that one of the charged

Received: November 6, 2020
Revised: January 8, 2021
Published: January 21, 2021

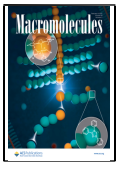

https://dx.doi.org/10.1021/acs.macromol.0c02493
Macromolecules 2021, 54, 1414−1424

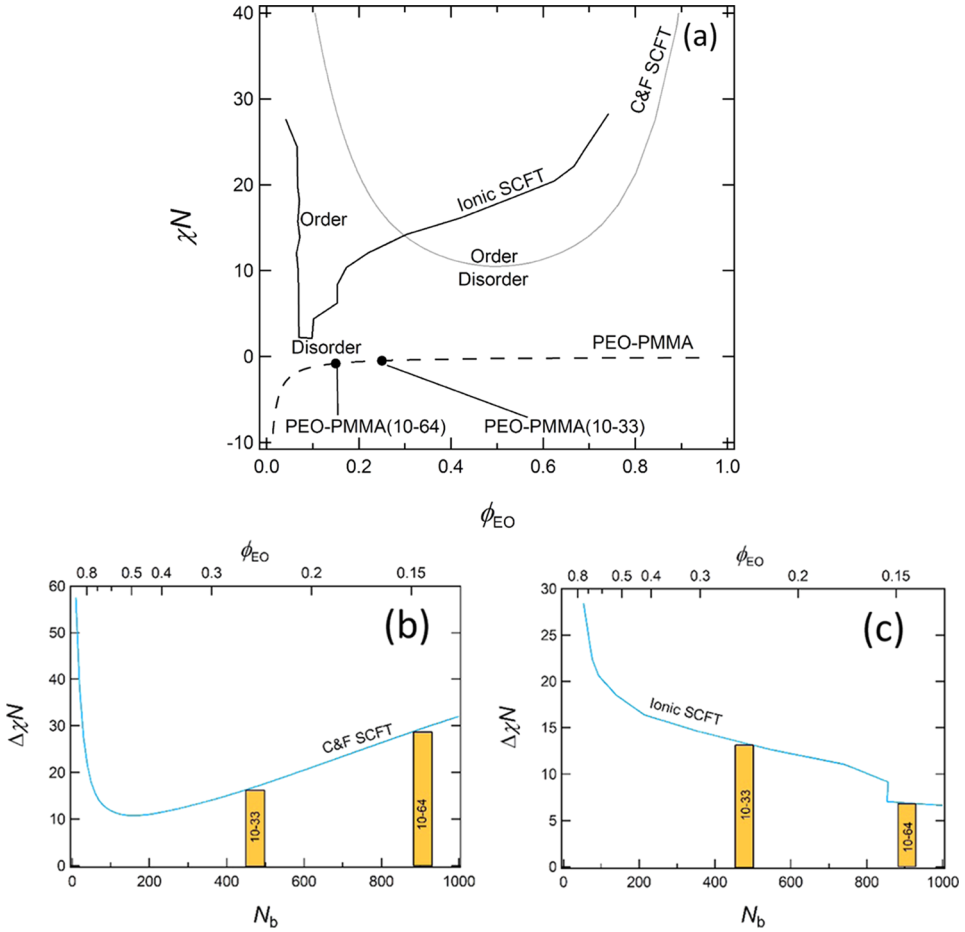

Figure 1. Phase diagrams for the PEO-PMMA block copolymer. Segregation strength, χN, is plotted as a function of the volume fraction of ethylene oxide, ϕ_{EO}, and the number of PMMA units, N_b. In (a), Fredrickson and Cochran order to disorder transition is plotted as the gray trace, as a function of ϕ_{EO}. The black trace is the ionic SCFT phase diagram by de la Cruz and co-workers. In (b), the change in segregation strength, $\Delta\chi N$, is shown between the classical phase diagram and the segregation strength of a PEO-PMMA block copolymer series with a 10 kg mol^{-1} block. Yellow bars mark the location of the two synthesized asymmetric block copolymers. In (c), the change in segregation strength, $\Delta\chi N$, is shown between the ionic SCFT phase diagram and the segregation strength of the PEO-PMMA block copolymer series.

species is covalently bonded to one block of the diblock copolymer.[18] In such systems if χ is small enough such that the disordered phase can be accessed, the driving force for order formation at constant N is largest at $\phi = 0.10$.

The main purpose of this work is to test the predictions of ionic SCFT. The system that we have studied is poly(ethylene oxide)-*b*-poly(methyl methacrylate) (PEO-PMMA) with added lithium bis(trifluoromethanesulfonyl)imide (LiTFSI) salt. Numerous studies have been conducted on PEO/PMMA homopolymer blends, since it is one of the few polymer blend systems that is completely miscible.[27−31] The value of χ between PEO and PMMA is -7.8×10^{-4} based on a reference volume of 0.1 nm^3, and it is independent of temperature.[32,33] A negative χ parameter is generally taken as a signature of attractive interactions between the blocks. We synthesized two block copolymers, starting with a 10 kg mol^{-1} PEO macroinitiator and then polymerizing methyl methacrylate via atom transfer radical polymerization.[34] We thus change ϕ in our system by keeping N_a, the number of repeat units in the PEO block, fixed at 154 and changing N_b, the number of repeat units in the PMMA block. The trajectory traversed by a series of block copolymers with $N_a = 154$ on the χN versus ϕ phase diagram is shown by a dashed curve in Figure 1a; a value of $\chi = -7.8 \times 10^{-4}$ was used to create the trajectory. This trajectory is located entirely within the disordered region of the classical block copolymer phase diagram. In other words, all block copolymers along this trajectory are predicted to be disordered regardless of temperature because χ is independent of temperature. The two polymers of interest have PEO volume fractions of $\phi = 0.15$ and 0.25, and they are represented by dots on this trajectory. The vertical distance between this trajectory and the order−disorder transition boundary is a measure of the driving force for order formation. This driving force quantified by $\Delta\chi N$ is plotted as a function N_b in Figure 1b. The driving force for order formation for the ionic SCFT phase diagram in Figure 1a is plotted using the same axes in Figure 1c. The bars in Figure 1b,c represent the driving force for order formation in the two polymers of interest. We note in passing that mapping experimental results onto the ionic phase diagram requires considerable effort[35] that goes beyond the scope of the present paper. While we have used a particular phase diagram taken from ref 18 to construct Figure 1, the same qualitative behavior would be seen if any of the other phase diagrams were used either from ref 18 or ref 20. If we hypothesize that the classical block copolymer phase diagram was applicable to PEO-PMMA/LiTFSI mixtures, then it would be easier to induce order in the copolymer with $\phi = 0.25$. In contrast, if we hypothesize that the ionic SCFT block

https://dx.doi.org/10.1021/acs.macromol.0c02493
Macromolecules 2021, 54, 1414−1424

copolymer phase diagram was applicable then it would be easier to induce order in a polymer with $\phi = 0.15$. Our main objective is to determine which hypothesis is correct.

Two series of block copolymer electrolytes were prepared, adding salt to the two PEO-PMMA block copolymers described above. We demonstrate that the magnitudes of the concentration fluctuations are larger in the more asymmetric PEO-PMMA polymer electrolyte. This finding, established using small-angle X-ray scattering (SAXS), lends considerable support to ionic SCFT. It is, perhaps, worth noting the difference between PEO-PMMA and the well-studied block copolymer, poly(ethylene oxide)-*b*-polystyrene (PEO-PS) electrolytes. The phase behavior of PEO-PS in the absence of salt is relatively simple: block copolymers with small chain lengths are disordered while those with large chain lengths are ordered.[10] For a symmetric diblock copolymer, the molar mass of PEO-PS that enables access to order−disorder transitions at reasonable temperatures is about 14 kg mol^{-1}.[25] It was relatively straightforward to synthesize polymers in this range of molar masses and study the effect of added salt.[25,26,36,37] A similar starting point for the study of PEO-PMMA electrolytes did not exist when we began this study. Specifically, there was no rational approach for deciding on the composition and chain length of PEO-PMMA block copolymers to begin investigating the effect of added salt on the thermodynamics of this system.

MATERIALS AND METHODS

Macroinitiator Synthesis. PEO (Sigma-Aldrich, molar mass = 10 kg mol^{-1}, 20 g, 2 mmol, 1 equiv, $Đ = 1.2$) was dissolved in a 250 mL round-bottom flask in dichloromethane (200 mL). *N*-(3-dimethylaminopropyl)-*N*′-ethylcarbodiimide hydrochloride (EDC·HCL, Carbosynth, 770 mg, 4 mmol, 2 equiv), 4-(dimethylamino)pyridine (DMAP, Sigma-Aldrich, 26 mg, 0.2 mmol, 10 mol %), and α-bromophenylacetic acid (BPAA, Combi-Blocks, 1.3 g, 6 mmol, 3 equiv) were added to the solution at room temperature. After 48 h, the solution was washed three times in a separatory funnel with a saturated solution of sodium bicarbonate and water at room temperature. The solution was dried over magnesium sulfate, concentrated in a rotary evaporator until viscous, and then reprecipitated in room-temperature diethyl ether.

PEO-PMMA Synthesis. PEO-PMMA block copolymer was synthesized via atom transfer radical polymerization (ATRP) using a macroinitiator comprising of a 10 kg mol^{-1} PEO chain with a α-bromophenylacetate terminus. The PEO-α-bromophenylacetate macroinitiator (1 equiv) was dissolved in degassed anisole at room temperature in a sealed 10 mL round-bottom flask. A copper wire (treated in a solution of HCl in methanol), $CuBr_2$ (0.02 equiv dissolved in dimethyl sulfoxide (DMSO)), *N*,*N*,*N*′,*N*″,*N*″-pentamethyldiethylenetriamine (PMDETA, 0.18 equiv), and methyl methacrylate monomer (purified by passing through a column of basic alumina and degassed by nitrogen sparging) were added to the reaction mixture. Two different PEO-PMMA block copolymers were synthesized by allowing the reaction to proceed for 18 and 24 h at room temperature. The reaction was stopped by dilution with tetrahydrofuran (THF) and subsequent passage through a basic alumina filter to remove the copper ions. The polymers were twice reprecipitated in water. Molar mass was determined with ^{1}H nuclear magnetic resonance (NMR) spectroscopy and the dispersity ($Đ$) was determined with gel permeation chromatography (GPC). The structure of PEO-PMMA is shown in Scheme 1. The neat copolymers are colorless. Exact quantities of reagents are found in the Supporting Information.

In this study, polymers are referred to as PEO-PMMA(x−y), where x and y are the molar masses of the respective blocks in kg mol^{-1}. The number of monomers per block was calculated by

Scheme 1. Chemical Structure of PEO_{10K}-PMMA

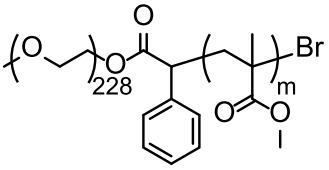

$$N_i = \frac{M_i}{\rho_i v_{ref}} \quad (1)$$

where v_{ref} is set to 0.1 nm^3. The total number of monomers for the block copolymer is given as

$$N = N_{PEO} + N_{PMMA} \quad (2)$$

The list of polymers used in this study is shown in Table 1.

Table 1. Polymer Properties

PEO-PMMA	M_{PEO} (kg mol^{-1})	M_{PMMA} (kg mol^{-1})	ϕ_{EO} 90 °C	N 90 °C	$Đ$
10−33	10	33	0.25	624	1.13
10−64	10	64	0.15	1065	1.21

The volume fraction of the neat copolymers is calculated by

$$\Phi_{EO} = \frac{v_{EO}}{v_{EO} + \frac{M_{PMMA}M_{EO}}{M_{MMA}M_{PEO}}v_{MMA}} \quad (3)$$

where ν_{EO} and ν_{MMA} are the molar volumes of ethylene oxide monomers and methyl methacrylate monomers, respectively, and M_{MMA} and M_{EO} are the molar masses of the respective monomers. Molar volumes are calculated by

$$v_i = \frac{M_i}{\rho_i} \quad (4)$$

where i = PEO, PMMA. We use subscripts of EO and MMA for properties of the monomer and subscripts of PEO and PMMA for properties of the polymeric blocks. The following expressions were used to calculate the density of PEO and PMMA as a function of temperature[38]

$$\rho_{PEO} = 1.139 - 7.31 \times 10^{-4} \times T \quad (5)$$

$$\rho_{PMMA} = 1.188 - 1.34 \times 10^{-4} \times T - 9.1 \times 10^{-7} \times T^2 \quad (6)$$

$$\rho_{PMMA} = 1.223 - 5.29 \times 10^{-4} \times T - 0.507 \times 10^{-6} \times T^2 \quad (7)$$

where eq 6 applies for 30 $< T$ (°C) $<$ 100 and eq 7 applies for 120 $< T$ (°C) $<$ 270.

^{1}H NMR. The composition of the PEO-PMMA block copolymers was determined using ^{1}H NMR ($CDCl_3$, Brucker AV400). The composition was calculated by integrating the ethylene proton peak at 3.64 ppm against the proton peak for the methyl group on the MMA repeat units at 1.02, 0.85, and 3.60 ppm.[39] The ^{1}H NMR profiles are shown in the Supporting Information.

Gel Permeation Chromatography. The PEO-PMMA block copolymers were characterized on an Agilent 1260 Infinity Series gel permeation chromatography (GPC) system with Waters Styragel HR3 and HR4 columns with a *N*-methyl-2-pyrrolidone (NMP) mobile phase with 0.05 M LiBr at 70 °C. The RI detector was utilized to calculate the polydispersity ($Đ = M_w/M_n$) based upon poly(ethylene oxide) calibration standards. The PEO precursor molar mass was determined to be 9.1 kg mol^{-1} ($Đ = 1.2$). NMR was utilized to calculate the molar mass and composition of the PEO-PMMA block copolymers; we used the molar mass of the PEO precursor provided by the manufacturer (10 kg mol^{-1}) in these calculations.

https://dx.doi.org/10.1021/acs.macromol.0c02493
Macromolecules 2021, 54, 1414−1424

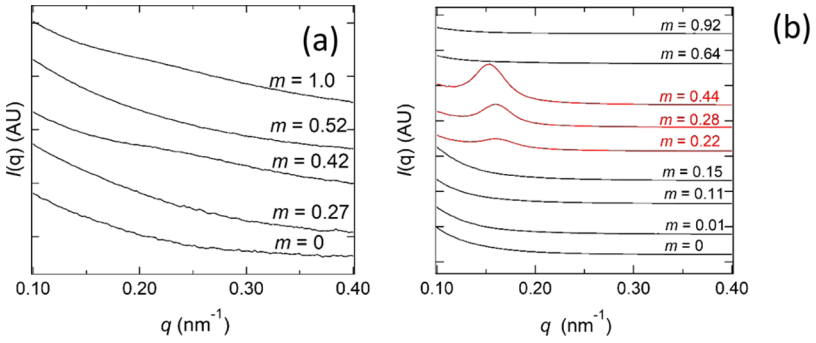

Figure 2. SAXS profiles of PEO-PMMA performed at ALS beamline 7.3.3. Scattering intensity is plotted as a function of the scattering vector, q. In (a), profiles are shown of PEO-PMMA(10−33) for a range of salt concentrations at 90 °C, offset vertically for clarity. In (b), profiles are shown for PEO-PMMA(10−64) for a range of salt concentrations at 90 °C. Salt concentration is given as m = mol Li/kg polymer. Red curves signify a disordered phase evidenced by a broad primary scattering peak at $q^* = 0.16$ nm^{-1}.

GPC traces of the PEO precursor and the block copolymers are shown in the Supporting Information.

Electrolyte Preparation. Electrolytes were made by mixing LiTFSI with each polymer in the presence of solvent. All electrolytes were prepared in an MBraun argon glovebox to prevent LiTFSI from complexing with water. Water and O_2 levels in the glovebox were kept below 1 and 0.1 ppm, respectively, during electrolyte preparation. Neat PEO-PMMA was dried under vacuum at 90 °C for 72 h in a glovebox antechamber before electrolyte preparation. The dry polymer and LiTFSI were placed in a scintillation vial and anhydrous THF was added to the mixture. The electrolyte was mixed at 60 °C for 2 h to ensure that both the polymer and salt were completely dissolved. After 2 h, the caps from the vials were removed, and the solvent was evaporated off at 60 °C for 12 h. The electrolytes were then transferred to a glovebox antechamber and placed under vacuum at 90 °C for 72 h to evaporate off any remaining THF. The dry electrolytes were clear and extremely hard and glassy at room temperature. The salt concentration in the electrolytes was quantified by molality (m), or the ratio of moles of lithium to kilograms of solvent or the polymer in this study.

Small-Angle X-Ray Scattering (SAXS) Measurements. SAXS samples were made by melt pressing the polymer into 1/16 in thick Viton spacers (McMaster Carr) with an inner diameter of 1/8 in at 140 °C in an MBraun argon glovebox. These spacers were placed in custom airtight aluminum sample holders with Kapton windows and annealed at 140 °C under vacuum for 48 h and then allowed to cool to room temperature for 24 h. These samples were placed in a custom 8-hole temperature-controlled motorized stage and annealed at each target temperature for 30 min before taking SAXS measurements. SAXS measurements were taken at beamline 7.3.3 at the Advanced Light Source at the Lawrence Berkeley National Lab and Stanford Synchrotron Radiation Light Source beamline 1-5 at the SLAC National Accelerator Laboratory.[40] Silver behenate was used to calculate the beam center and the sample-to-detector distance. The scattering intensity was corrected for air gaps, empty cell scattering, and beam transmission. A glassy carbon standard provided by NIST was used to convert the beam intensity into absolute intensity. The Nika program in Igor Pro was used to azimuthally integrate two-dimensional (2D) scattering patterns into one-dimensional scattering patterns.[41]

RESULTS AND DISCUSSION

The measured SAXS profiles of PEO-PMMA(10−33) and PEO-PMMA(10−64) electrolytes at a fixed temperature of 90 °C are shown in Figure 2. Both systems exhibit featureless SAXS profiles in the neat state. For PEO-PMMA(10−33), the addition of salt has no qualitative impact on the SAXS profiles; they are featureless across the salt concentration range $0 \leq m \leq 1.0$ mol Li/kg polymer. In contrast, PEO-PMMA(10−64) exhibits a well-defined scattering peak at $q = q^* = 0.16$ nm^{-1} in the salt concentration window $0.22 \leq m \leq 0.44$ mol Li/kg polymer. The peak increases in intensity as m is increased from 0.22 to 0.44. Further increase in salt concentration from m = 0.44 mol Li/kg polymer to m = 0.92 mol Li/kg polymer results in a featureless SAXS profile. The scattering peaks in Figure 2b are due to the emergence of concentration fluctuations that are announcements of a disorder-to-order transition.[1,4] This announcement is only detected in PEO-PMMA(10−64).

If the thermodynamics of PEO-PMMA/LiTFSI mixtures could be explained on the basis of conventional block copolymer SCFT, then PEO-PMMA(10−33) would be closer to the disorder-to-order transition (Figure 1b). Instead, we see that PEO-PMMA(10−64) is closer to the disorder-to-order transition due to the presence of the SAXS peaks, consistent with the predictions of ionic SCFT (Figure 1c).

The scattering profiles in Figure 2 were converted to absolute intensity, as detailed in the Materials and Methods section. The total intensities of scattering profiles with a disordered peak are given as

$$I_{tot}(q) = I_{dis}(q) + I_{bkgd}(q) \tag{8}$$

where $I_{bkgd}(q)$ is the background and $I_{dis}(q)$ is the intensity of the disordered peak. $I_{bkgd}(q)$ is assumed to be an exponentially decaying function of q, with two adjustable parameters.[25] Figure 3 plots the background-subtracted scattering profiles of the PEO-PMMA(10−64) m = 0.22, 0.28, and 0.44 mol Li/kg

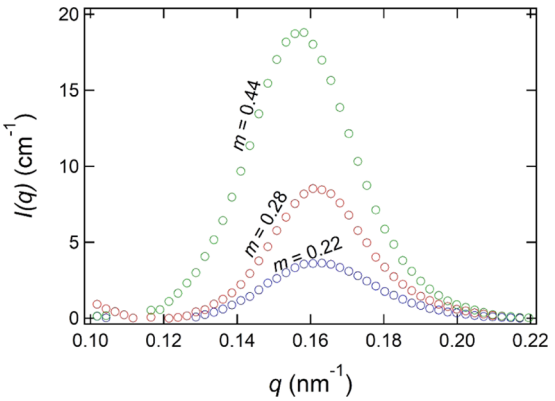

Figure 3. Background-subtracted absolute intensity SAXS profiles of PEO-PMMA(10−64) m = 0.22, 0.28, and 0.44 mol Li/kg polymer plotted as a function of the scattering vector, q. These profiles were taken at 90 °C.

https://dx.doi.org/10.1021/acs.macromol.0c02493
Macromolecules 2021, 54, 1414−1424

polymer electrolytes at 90 °C, the only three electrolytes that exhibit scattering peaks.

There are no explicit theoretical predictions for the scattering profiles of disordered mixtures of salt and block copolymers that we could use to analyze our data. Lacking a better alternative, we use the random phase approximation (RPA) to interpret the measured scattering profiles; this is similar to the approach used in the study of other disordered block copolymer/salt mixtures.[25,36,42−44] The RPA theory predicts the absolute scattering intensity of a monodisperse AB diblock copolymer

$$I_{dis}(q) = C\left[\frac{S(q)}{W(q)} - 2\chi_{eff}\right]^{-1} \tag{9}$$

where C is the X-ray scattering contrast that is governed by electron density differences.[1] The parameter χ_{eff} is the effective Flory−Huggins interaction parameter that describes interactions between PEO/LiTFSI and PMMA/LiTFSI units. $W(q)$ and $S(q)$ are the determinant and the sum of the structure factor matrix $\|S_{ij}\|$. The expressions for $W(q)$ and $S(q)$ are given by

$$W(q) = S^{\circ}_{AA}S^{\circ}_{BB} - (S^{\circ}_{AB})^2 \tag{10}$$

$$S(q) = S^{\circ}_{AA} + S^{\circ}_{BB} + 2S^{\circ}_{AB} \tag{11}$$

where

$$S^{\circ}_{ii} = f_i N_i \nu_i P_i(q) (i = A, B) \tag{12}$$

$$S^{\circ}_{AB} = S^{\circ}_{BA} = (N_A f_A N_B f_B)^{1/2} F_A(q) F_B(q) \tag{13}$$

and

$$P_i(q) = 2\left[\frac{\exp(-x_i) - 1 + x_i}{x_i^2}\right] \tag{14}$$

$$F_i = \frac{1 - \exp(-x_i)}{x_i} \tag{15}$$

with $x_i = q^2 R_{g,i}^2$. Each block is modeled as a Gaussian chain and

$$R_{g,i}^2 = \frac{N_i(\alpha a_i)^2}{6} (i = PMMA, PEO) \tag{16}$$

where a_i is the respective statistical segment length of the block. In this study, we set a_{PEO}= 0.72 and a_{PMMA} = 0.54.[38] In eq 16, α represents the chain stretching parameter accounting for the difference between the experimental values of R_g and those based on the statistical segment lengths reported in ref 38. N_i in eqs 12, 13, and 16 is the number of repeat units in block i based on a ν_{ref} of 0.1 nm^3. Equations 9−16 are used to calculate the scattering profiles for disordered block copolymer electrolytes.

As described in eq 9, the intensity of the disordered peak is both a function of χ_{eff} and contrast. The contrast in neat systems quantifies the difference in electron density in the two blocks of the block copolymer and is given by

$$C_{neat} = \left(\frac{b_{EO}}{\nu_{EO}} - \frac{b_{MMA}}{\nu_{MMA}}\right)^2 \tag{17}$$

where b_{EO} and b_{MMA} are the respective X-ray scattering lengths of the two components based on pure component densities.

As seen in Figure 3, peak intensity increases as salt concentration increases. Increasing peak intensity can correspond to either an increase in χ or an increase in contrast. In block copolymer electrolytes, the contrast depends crucially on salt distribution between the two blocks. If we assume that the salt preferentially segregates in the PEO fluctuations, contrast is given by

$$C_{PEO-salt} = \nu_{ref}\left(\frac{b_{EO} + \left(\frac{n_{LiTFSI}}{n_{EO}}\right)b_{LiTFSI}}{\nu_{EO} + \left(\frac{n_{LiTFSI}}{n_{EO}}\right)\nu_{LiTFSI}} - \frac{b_{MMA}}{\nu_{MMA}}\right)^2 \tag{18}$$

where n_{EO} is the number of ethylene oxide monomers per chain.[25] At the other extreme, one might assume that salt is uniformly distributed in both kinds of fluctuations and in this case, the contrast is given by

$$C_{uniform\ salt} = \Phi_{polymer}\left(\frac{b_{EO}}{\nu_{EO}} - \frac{b_{MMA}}{\nu_{MMA}}\right)^2 \tag{19}$$

where $\Phi_{polymer}$ is the overall volume fraction of the polymer in the polymer−salt mixture.[45] The final option is an adjustable contrast model, first developed by Chintapalli et al., wherein C depends on the partitioning of LiTFSI between the PEO-rich and the PMMA-rich concentration fluctuations.[46] This partitioning is quantified by a salt affinity fit parameter, γ, which can vary between 0 and 1. The expression for contrast is

$$C(\gamma) = \nu_{ref}\left(\frac{b_{EO} + p(\gamma)\left(\frac{n_{LiTFSI}}{n_{EO}}\right)b_{LiTFSI}}{\nu_{EO} + p(\gamma)\left(\frac{n_{LiTFSI}}{n_{EO}}\right)\nu_{LiTFSI}} - \frac{b_{MMA} + (1 - p(\gamma))\left(\frac{n_{LiTFSI}}{n_{MMA}}\right)b_{LiTFSI}}{\nu_{MMA} + (1 - p(\gamma))\left(\frac{n_{LiTFSI}}{n_{MMA}}\right)\nu_{LiTFSI}}\right)^2 \tag{20}$$

where n_{MMA} is the number of MMA monomers per chain, calculated as $n = M_{polymer}/M_{monomer}$, and b_{EO}, b_{MMA}, and b_{LiTFSI} are the respective X-ray scattering lengths of the three components based on pure component densities.[46] In eq 20, p is given by

$$p(\gamma) = \frac{n_{EO}\gamma}{n_{EO}\gamma + n_{MMA}(1 - \gamma)} \tag{21}$$

The parameter γ reflects how favorable the LiTFSI−EO interaction is relative to the LiTFSI−MMA interaction: it is the probability that an LiTFSI molecule will associate with an EO monomer when given the choice between EO or MMA. In the case where $n_{EO} = n_{MMA}$, $p(\gamma) = \gamma$. Thus, $p(\gamma)$ represents the fraction of LiTFSI in the PEO-rich fluctuations.

An important parameter is the volume fraction of the PMMA-rich fluctuation in the presence of salt. This is given by

$$\Phi_{MMA}(\gamma) = \frac{n_{MMA}\nu_{MMA} + (1 - p(\gamma))n_{LiTFSI}\nu_{LiTFSI}}{n_{MMA}\nu_{MMA} + n_{LiTFSI}\nu_{LiTFSI} + n_{EO}\nu_{EO}} \tag{22}$$

Figure 4 plots the best fits of eq 9 through the data of PEO-PMMA(10−64)/LiTFSI with m = 0.44 mol Li/kg polymer at 90 °C with χ_{eff} and α as adjustable variables. We begin by comparing the predictions using the contrast calculated with the uniform salt assumption (eq 19). This fit overestimates the peak intensity and underestimates the intensity in the wings.

https://dx.doi.org/10.1021/acs.macromol.0c02493
Macromolecules 2021, 54, 1414−1424

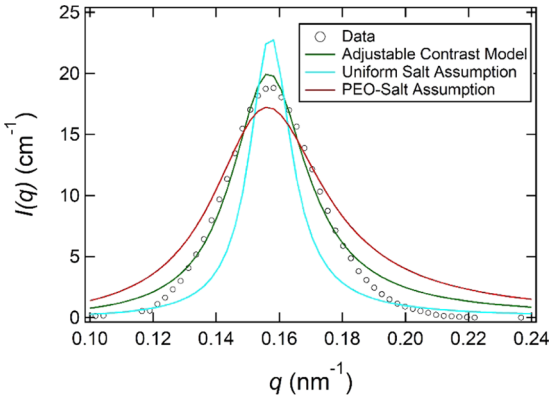

Figure 4. Circles represent data of PEO-PMMA(10−64)/LiTFSI with m = 0.44 mol Li/kg polymer at 90 °C. The curves represent best fits using three different models with χ_{eff} as the main adjustable parameter.

Next, we compare predictions using the contrast calculated with the PEO−salt assumption (eq 18). This fit underestimates the peak intensity and overestimates the intensity in the wings. The lack of agreement between these two fitting procedures indicates that the salt ions are neither completely segregated in the PEO-rich fluctuations nor uniformly dispersed between the PEO-rich and PMMA-rich fluctuations. We are thus forced to use the adjustable contrast model (eqs 20−22) with χ_{eff}, α, and γ as adjustable fit parameters. We find quantitative agreement between the experimental data and this model. The chain stretching parameter, α, ranges between 1.68 and 1.74, as reported in the Supporting Information (between 1.68 and 1.74). These values are larger than those for PEO-PS/LiTFSI mixtures, which range between 0.8 and 1.4.[42]

Figure 5a shows background-subtracted scattering profiles of PEO-PMMA(10−64) for the m = 0.22 mol Li/kg polymer electrolyte from 70 to 150 °C. When the temperature is increased from 70 to 90 °C, the peak intensity decreases from 6 to 3.5 cm^{-1}: the peak at 90 °C is slightly narrower than the peak at 70 °C. The peak intensity is insensitive to a temperature between 90 and 130 °C, but a slight narrowing is evident with increasing temperature. Further increase of temperature from 130 to 150 °C results in a decrease in peak intensity to 3 cm^{-1} and a slight decrease in peak width. In pure copolymer melts, a decrease in peak intensity is a signature of a decrease in χ (C is fixed).[11,47] However, this decrease is generally a smooth function of temperature. Changes in the scattering profiles in Figure 5a, which are not smooth, may occur due to changes in C or χ_{eff}. We fitted the data to the adjustable contrast model to distinguish between these two effects. In Figure 5b, we compare experimental data with fits. It is evident that the complex trends seen in Figure 5a are captured by our model, provided χ_{eff}, α, and γ are used as adjustable parameters. This fitting procedure was applied to scattering curves at m = 0.22, 0.28, and 0.44 mol Li/kg polymer for all temperatures. The dependence of χ_{eff} on 1000/T for different salt concentrations is shown in Figure 6a. The data obtained at the given salt concentration is consistent with the expression often used to describe the temperature dependence of the Flory−Huggins interaction parameter

$$\chi_{eff} = \frac{A}{T} + B \tag{23}$$

The solid lines in Figure 6a are the fits for each salt concentration based upon eq 23 and are used to extract the A and B parameters. The parameters A and B thus obtained are shown in Table 2. χ_{eff} decreases with increasing temperature, implying that A is positive. The values of A obtained at different salt concentrations are within experimental error; the lines in Figure 6a are nearly parallel. The parameter B decreases with salt concentration, as shown in Table 2.

It is noteworthy that χ_{eff} is a smooth function of temperature at m = 0.22 mol Li/kg polymer (Figure 6a), despite the fact that the peak intensity is not a smooth function of temperature (Figure 5a). This conclusion was only reached after the partitioning of LiTFSI was accounted for. At this salt concentration, p lies within a narrow window of 0.90 and 1.0. In other words, most of the LiTFSI is associated with the PEO-rich fluctuations. However, accounting for the small concentration of LiTFSI in the PMMA-rich fluctuations is crucial for quantitative analysis of the SAXS data. The partitioning of salt in the PMMA-rich fluctuations increases with increasing salt concentration, as seen in Figure 6b. The smallest values of p are obtained at m = 0.44 mol Li/kg polymer: they lie between 0.86 and 0.80. The dependence of p on temperature varies qualitatively with salt concentration. The dependence of α on m and T is given in the Supporting Information (Figure S3).

Figure 7 shows χ_{eff} plotted as a function of salt concentration at 90 °C. For the three salt concentrations at which χ_{eff} values were measured explicitly, χ_{eff} decreases more-or-less linearly

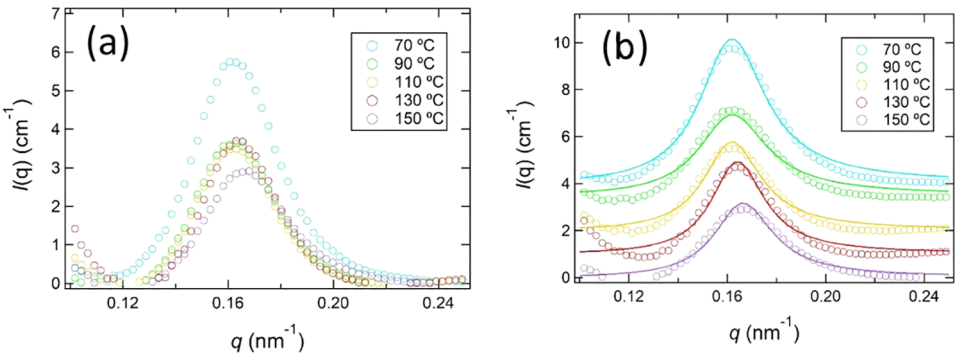

Figure 5. In (a), background-subtracted scattering profiles of the PEO-PMMA(10−64) m = 0.22 mol Li/kg polymer electrolyte are plotted as a function of the scattering vector, q, from 70 to 150 °C. In (b), the RPA fits for each scattering profile of the PEO-PMMA(10−64) m = 0.22 mol Li/kg polymer electrolyte are plotted against the background-subtracted data as a function of the scattering vector, q, from 70 to 150 °C. The absolute $I(q)$ for T = 150 °C is presented. Data from 130, 110, 90, and 70 °C are shifted vertically by 1, 2, 3.5, and 4 cm^{-1}, respectively, for clarity.

https://dx.doi.org/10.1021/acs.macromol.0c02493
Macromolecules 2021, 54, 1414−1424

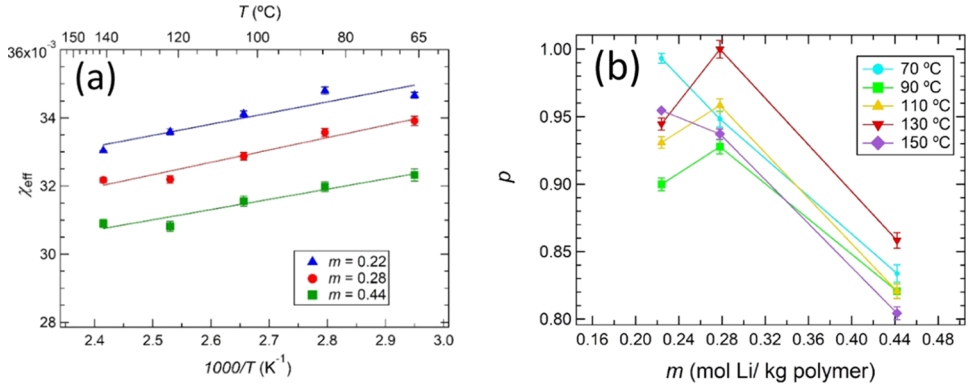

Figure 6. In (a), χ_{eff} is plotted against inverse temperature to calculate χ_{eff} as a function of temperature at each salt concentration with a disordered peak. Fit parameters can be seen in Table 2. In (b), the fraction of lithium salt in PEO fluctuation (p) as derived from RPA fits is plotted as a function of salt concentration. Each trace represents a temperature from SAXS measurements.

Table 2. χ_{eff} Fit Parameters

m (mol Li/kg polymer)	$A \times 10^3$ (K)	B	R^2
0.22	3.2 ± 0.68	0.025 ± 0.0018	0.89
0.28	3.6 ± 0.46	0.023 ± 0.0012	0.95
0.44	3.0 ± 0.46	0.024 ± 0.0012	0.93

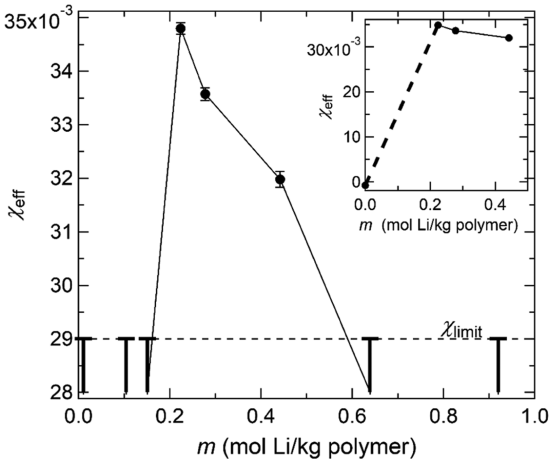

Figure 7. χ_{eff} is plotted as a function of salt concentration at 90 °C. The error bars represent the minimum χ value required for a disordered peak. The inset plots the three calculated χ_{eff} with the negative χ parameter from Russell and co-workers for a neat PEO-PMMA system.[33] The dotted line represents χ_{limit} or the minimum χ parameter required to observe a disordered peak.

with increasing m. However, the SAXS data obtained at other salt concentrations indicates a more complex relationship between χ_{eff} and m. In any SAXS experiment on disordered block copolymers, χ_{eff} can only be determined if scattering from the disordered phase rises above the background. Since the scattering intensity increases monotonically with increasing χ_{eff}, there is an upper limit on the value of χ_{eff} that can be measured. We systematically changed χ_{eff}, calculated $I_{dis}(q)$ using eqs 9−16, and found that when $\chi_{eff} = \chi_{limit} = 0.029$ the magnitude of $I_{dis}(q^*)$ is a factor of 1.06 above $I_{bkgd}(q^*)$. In other words, if χ_{eff} were less than or equal to χ_{limit} then the scattering signature of disordered fluctuations would be undetectable. We know that this is the case for PEO-PMMA/LiTFSI mixtures with the m < 0.22 mol Li/kg polymer and m > 0.44 mol Li/kg polymer; see scattering profiles in these salt concentration ranges in Figure 2. For completeness, we also show χ_{limit} at the salt concentrations where no SAXS peaks were detectable in Figure 7. The lines in Figure 7 connect adjacent data points. The data in Figure 7 reveal that χ_{eff} is a nonmonotonic function of m. Below m = 0.22 mol Li/kg polymer, χ_{eff} increases with added salt. Above m = 0.44 mol Li/kg polymer, χ_{eff} decreases with added salt. It is known that χ between PMMA and PEO in the absence of salt is -7.8×10^{-4}.[32,33] Our observation of increasing χ_{eff} with added salt in the low-salt-concentration regime is consistent with this result, as shown in the inset of Figure 7. The nonmonotonic relationship between χ_{eff} and salt concentration may be explained by a competition between ion solvation, screening, and entropic effects.[17,23,42,48] At low salt concentrations, ion solvation effects dominate, which drives ordering, while at high salt concentrations, entropic effects dominate, which drives disordering. Above m = 0.44 mol Li/kg polymer, χ_{eff} decreases with added salt. We posit that the lack of scattering peaks in samples with m > 0.44 mol Li/kg polymer in PEO-PMMA(10−64) seen in Figure 2b is attributed to the fact that χ_{eff} is below χ_{limit} (0.029). We will return to this point shortly.

Our definition of χ_{limit} is affected by our choice of two parameters: (1) The assumption that a disordered SAXS peak is detectable when $I_{dis}(q^*)$ is 6% higher than $I_{bkgd}(q^*)$ and (2) the exact value of m chosen for the calculation. If we assume that the disordered SAXS peak is detectable when $I_{dis}(q^*)$ is 10% higher than $I_{bkgd}(q^*)$, χ_{limit} would be 0.0315. If we change the value of m to the 0.44 mol Li/kg polymer to calculate χ_{limit}, then χ_{limit} is 0.020. Our main conclusions based on the data in Figure 7 are unaffected by the particular values we have chosen for these parameters.

In the field of block copolymer electrolytes,[11,36,37,49−52] it is customary to plot χ_{eff} as a function of salt concentration, as we have done in Figure 7. For example, in the case of PEO-PS block copolymer systems, it is customary to plot χ_{eff} as a function of r, the molar ratio of lithium ions and ethylene oxide monomers (r = [Li]/[EO]).[11,37,51] The implicit assumption in such plots is that the salt resides exclusively in the PEO-rich fluctuations. For the case PEO-PMMA/LiTFSI, it is important to show χ_{eff} as a function of salt concentration in both PEO-rich and PMMA-rich fluctuations. Using p, we can calculate the amount of lithium in the PEO-rich and PMMA-rich fluctuations as given by

https://dx.doi.org/10.1021/acs.macromol.0c02493
Macromolecules 2021, 54, 1414−1424

$$r = \frac{p[\mathrm{Li}]}{[\mathrm{EO}]} \tag{24}$$

and

$$z = \frac{(1-p)[\mathrm{Li}]}{[\mathrm{MMA}]} \tag{25}$$

In Figure 8, we plot χ_{eff} at 90 °C as a function of r and z. The thermodynamic properties of PEO-PMMA/LiTFSI mixtures as a function of added salt are described by a trajectory of χ_{eff} as a function of r and z. χ_{eff} is a monotonically decreasing function of r but a nonmonotonic function of z. At the highest salt concentration studied, the value of r in the PEO-rich fluctuations is 0.15. As this concentration is approached, the value of z increases substantially, suggesting a large driving force for LiTFSI to reside in PMMA-rich fluctuations. It is known that in mixtures of homopolymer PEO and LiTFSI lithium ions are coordinated with six ether oxygens, corresponding with $r = 1/6 = 0.16$.[53−55] The data in Figure 8 suggests that salt partitioning into the PMMA-rich fluctuations becomes significant when this concentration is reached in the PEO-rich fluctuations. Unfortunately, the systems investigated thus far have only revealed a small portion of χ_{eff} as a function of r and z, limiting the conclusions that can be drawn on the mechanisms underlying LiTFSI partition. Despite this limitation, the data shown in Figures 6−8 provide a starting point for quantifying the effect of added salt on PEO-PMMA block copolymers.

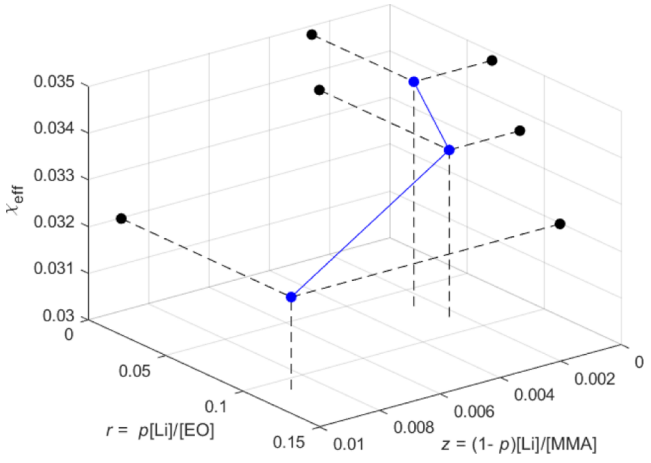

Figure 8. χ_{eff} plotted as a function of salt concentrations $r = p[\mathrm{Li}]/[\mathrm{EO}]$ and $z = (1-p)[\mathrm{Li}]/[\mathrm{MMA}]$. The blue trace is measured χ_{eff} as a function of both salt concentrations.

The most nonintuitive result of our study is contained in Figure 2b, where we see that the addition of salt leads to an emergence of a scattering peak that increases in intensity up to m = 0.44 mol Li/kg polymer: further increase in salt concentration to m = 0.64 mol Li/kg polymer results in the disappearance of this peak. To understand this result, we need to quantify the dependence of scattering contrast on m. In Figure 9a, we show the scattering length densities of PMMA/LiTFSI and PEO/LiTFSI mixtures as a function of added salt, z and r. The two circles on each curve represent the values of r and z that are covered in this study. The SAXS intensity is affected by the vertical distance between the corresponding points, as shown in Figure 9a: C is given by the square of this distance. For completeness, in Figure 9b, we plot C as a function of m, which is affected by the dependence of p on m, which is also shown in the figure. Here, we see that C increases monotonically as a function of m despite the fact that salt partitioning, p, decreases with m. We expect the contrast between PMMA-rich and PEO-rich fluctuations to increase with increasing m. We can thus assert that the lack of a scattering peak at m = 0.64 mol Li/kg polymer is not due to a lack of contrast but a decrease in χ_{eff}. The increase in peak intensity with salt concentration seen in Figure 3 is entirely due to an increase in contrast. In fact, χ_{eff} decreases with salt concentration.

CONCLUSIONS

In this paper, we described the synthesis and characterization of PEO-PMMA block copolymer electrolytes. The polymers were synthesized using a macroinitiator comprising of a 10 kg mol^{-1} PEO chain with a α-bromophenylacetate terminus. The targeted PMMA block was then obtained via ATRP. The thermodynamic interactions between PEO and PMMA were previously characterized by Ito et al. based on SANS experiments on blends containing deuterated PMMA.[33] The Flory−Huggins interaction parameter between PEO and PMMA is negative, implying that single-phase systems would be obtained regardless of composition, chain length, and temperature. Thermodynamic interactions in polymer blends and block copolymers can readily be determined by studying scattering from homogeneous systems that are close to phase

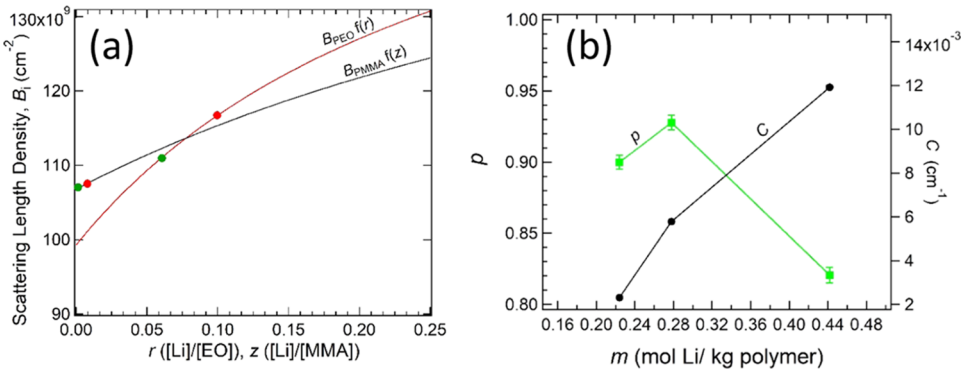

Figure 9. In (a), scattering length densities (B_i) for PEO and PMMA are plotted as a function of r and z. The circles on each curve represent the calculated salt concentrations covered within this study. The green circles show the lowest end of the salt concentration and the red circles show the highest end. In (b), p and contrast are plotted as a function of salt concentration (m) at 90 °C.

https://dx.doi.org/10.1021/acs.macromol.0c02493
Macromolecules 2021, 54, 1414−1424

boundaries. In these systems, the measured scattering profiles contain signatures of concentration fluctuations that may be considered as announcements of phase transitions. The challenge was to design PEO-PMMA block copolymers that would exhibit these signatures in the presence of added salt. We addressed this challenge by studying two series of mixtures of PEO-PMMA block copolymers and LiTFSI using SAXS.

The SAXS profiles of PEO-PMMA(10−33) were featureless in the neat state and at all salt concentrations. This series of mixtures provided no information on the effect of salt on the thermodynamic interactions between PEO and PMMA. The SAXS profiles of a more asymmetric block copolymer, PEO-PMMA(10−64), exhibited signatures of concentration fluctuations at intermediate salt concentrations. Featureless SAXS profiles were obtained in this series at both low and high salt concentrations. Conventional thermodynamic models of uncharged block copolymer systems lead to the conclusion that signatures of order formation should be suppressed in more asymmetric block copolymers. However, ionic SCFT first developed by de la Cruz and co-workers[18] indicates that added salt would enhance the signatures of order formation in more asymmetric block copolymers. Our results provide substantial support for the validity of ionic SCFT.

Direct mapping of experimental data on ionic SCFT predictions is nontrivial and has only been done in the case of the well-studied PEO-PS electrolytes.[35] This mapping was possible due to the availability of numerous experimental studies on concentration fluctuations in disordered mixtures of PEO-PS/LiTFSI and determination of phase boundaries in weakly ordered systems. The limited data we currently have on PEO-PMMA/LiTFSI mixtures precludes such mapping. Our analysis is thus based on using the SAXS profiles to estimate χ_{eff} using Leibler's random phase approximation. Our fitting procedure is an extension of previous work on PEO-PS electrolytes,[25] accounting for the partitioning of salt between the PEO and PMMA phases. In PEO-PMMA/LiTFSI mixtures we show that χ_{eff} is a complex nonmonotonic function of added salt. Such complexities may arise due to the interplay between ion solvation, screening, and entropy.[17,23,42,48] The dependence of thermodynamic interactions on added salt is thus presented on a three-dimensional plot that accounts for the partitioning of the salt between the PEO-rich and the PMMA-rich concentration fluctuations (Figure 8).

Our work lends considerable support to ionic SCFT and related models that account for polymer−ion interactions for thermodynamic predictions of phase behavior.[18−20] It also provides a foundation for designing microphase-separated block copolymer electrolytes in systems wherein the blocks exhibit attractive interactions with each other in the absence of salt, a foundation that did not exist when we began this study.

■ ASSOCIATED CONTENT

Supporting Information

The Supporting Information is available free of charge at https://pubs.acs.org/doi/10.1021/acs.macromol.0c02493.

NMR and GPC characterization data for PEO-PMMA block copolymers, further details about the polymer synthesis, α values for RPA fits, and secondary RPA fit results accounting for PDI of block copolymers used in this study (PDF)

■ AUTHOR INFORMATION

Corresponding Author

Nitash P. Balsara − *Department of Chemical and Biomolecular Engineering, University of California, Berkeley, Berkeley, California 94720, United States; Materials Sciences Division, Lawrence Berkeley National Laboratory, Berkeley, California 94720, United States;* orcid.org/0000-0002-0106-5565; Email: nbalsara@berkeley.edu

Authors

Neel J. Shah − *Department of Chemical and Biomolecular Engineering, University of California, Berkeley, Berkeley, California 94720, United States; Materials Sciences Division, Lawrence Berkeley National Laboratory, Berkeley, California 94720, United States;* orcid.org/0000-0002-2503-048X

Sajjad Dadashi-Silab − *Department of Chemistry, Carnegie Mellon University, Pittsburgh, Pennsylvania 15213, United States;* orcid.org/0000-0002-4285-5846

Michael D. Galluzzo − *Department of Chemical and Biomolecular Engineering, University of California, Berkeley, Berkeley, California 94720, United States; Materials Sciences Division, Lawrence Berkeley National Laboratory, Berkeley, California 94720, United States;* orcid.org/0000-0002-5776-0540

Saheli Chakraborty − *Energy Storage and Distributed Resources Division, Lawrence Berkeley National Laboratory, Berkeley, California 94720, United States;* orcid.org/0000-0003-0928-7020

Whitney S. Loo − *Department of Chemical and Biomolecular Engineering, University of California, Berkeley, Berkeley, California 94720, United States; Materials Sciences Division, Lawrence Berkeley National Laboratory, Berkeley, California 94720, United States;* orcid.org/0000-0002-9773-3571

Krzysztof Matyjaszewski − *Department of Chemistry, Carnegie Mellon University, Pittsburgh, Pennsylvania 15213, United States;* orcid.org/0000-0003-1960-3402

Complete contact information is available at: https://pubs.acs.org/10.1021/acs.macromol.0c02493

Notes

The authors declare no competing financial interest.

■ ACKNOWLEDGMENTS

This research was supported by the National Science Foundation grant DMR 1904508 to the University of California, Berkeley, and CHE 2000391 to Carnegie Melon University. This research used resources of the Advanced Light Source, a U.S. DOE Office of Science User Facility under Contract No. DE-AC02-05CH11231. Experiments conducted at the Stanford Synchrotron Radiation Light Source, SLAC National Accelerator Laboratory, are supported by the U.S. Department of Energy, Office of Science, Office of Basic Energy Sciences under Contract No. DE-AC02-76SF00515.

■ NOMENCLATURE

a_i	statistical segment length of species i (nm)
b_i	X-ray scattering length of species i (nm mer^{-1})
C	electron density contrast (cm^{-1})
$Đ$	dispersity
$I(q)$	scattering intensity (cm^{-1})
$I_{\text{dis}}(q)$	disordered scattering intensity (cm^{-1})
$I_{\text{bkgd}}(q)$	background scattering intensity (cm^{-1})

$I_{tot}(q)$ total scattering intensity (cm^{-1})
M_i molar mass of species i (g mol^{-1})
M_w weight-averaged molar mass (kg mol^{-1})
M_n number-averaged molar mass (kg mol^{-1})
M_{PEO} molar mass of species poly(ethylene oxide) (g mol^{-1})
M_{PMMA} molar mass of species poly(methyl methacrylate) (g mol^{-1})
m molality (mol Li/kg polymer)
n_i chemical repeat units for species i
N degree of polymerization
N_i degree of polymerization for species i
p fraction of lithium in ethylene oxide fluctuation
q scattering vector (nm^{-1})
q^* scattering vector at the primary scattering peak (nm^{-1})
r salt concentration in PEO ([Li] $[EO]^{-1}$)
R_g radius of gyration (nm)
T temperature (°C)
z salt concentration in PMMA ([Li] $[MMA]^{-1}$)

GREEKS

γ affinity parameter between salt and polymer fluctuation
ν_i molar volume of species i (cm^3 mol^{-1})
ν_{ref} reference volume of species i (cm^3 mol^{-1})
ρ_i density of species i (g cm^{-1})
ϕ_i volume fraction of species i
χ Flory–Huggins interaction parameter
χ_{eff} Flory–Huggins interaction parameter of PEO-PMMA/LiTFSI

REFERENCES

(1) Leibler, L. Theory of Microphase Separation in Block Copolymers. *Macromolecules* **1980**, *13*, 1602–1617.
(2) Gunkel, I.; Stepanow, S.; Thurn-Albrecht, T.; Trimper, S. Fluctuation Effects in the Theory of Microphase Separation of Diblock Copolymers in the Presence of an Electric Field. *Macromolecules* **2007**, *40*, 2186–2191.
(3) Cochran, E. W.; Garcia-Cervera, C. J.; Fredrickson, G. H. Stability of the Gyroid Phase in Diblock Copolymers at Strong Segregation. *Macromolecules* **2006**, *39*, 2449–2451.
(4) Fredrickson, G. H.; Helfand, E. Fluctuation Effects in the Theory of Microphase Separation in Block Copolymers. *J. Chem. Phys.* **1987**, *87*, 697–705.
(5) Chanpuriya, S.; Kim, K.; Zhang, J.; Lee, S.; Arora, A.; Dorfman, K. D.; Delaney, K. T.; Fredrickson, G. H.; Bates, F. S. Cornucopia of Nanoscale Ordered Phases in Sphere-Forming Tetrablock Terpolymers. *ACS Nano* **2016**, *10*, 4961–4972.
(6) Lee, S.; Leighton, C.; Bates, F. S. Sphericity and Symmetry Breaking in the Formation of Frank-Kasper Phases from One Component Materials. *Proc. Natl. Acad. Sci. U.S.A.* **2014**, *111*, 17723–17731.
(7) Liu, M.; Qiang, Y.; Li, W.; Qiu, F.; Shi, A. C. Stabilizing the Frank-Kasper Phases via Binary Blends of AB Diblock Copolymers. *ACS Macro Lett.* **2016**, *5*, 1167–1171.
(8) Matsen, M. W.; Schick, M. Stable and Unstable Phases of a Diblock Copolymer Melt. *Phys. Rev. Lett.* **1994**, *72*, No. 2660.
(9) Bates, F. Block Copolymer Thermodynamics: Theory And Experiment. *Annu. Rev. Phys. Chem.* **1990**, *41*, 525–557.
(10) Floudas, G.; Vazaiou, B.; Schipper, F.; Ulrich, R.; Wiesner, U.; Iatrou, H.; Hadjichristidis, N. Poly(Ethylene Oxide-b-Isoprene) Diblock Copolymer Phase Diagram. *Macromolecules* **2001**, *34*, 2947–2957.
(11) Ruzette, A.-V. G.; Soo, P. P.; Sadoway, D. R.; Mayes, A. M. Melt-Formable Block Copolymer Electrolytes for Lithium Rechargeable Batteries. *J. Electrochem. Soc.* **2001**, *148*, A537–A543.
(12) Soo, P. P.; et al. Rubbery Block Copolymer Electrolytes for Solid-State Rechargeable Lithium Batteries. *J. Electrochem. Soc.* **1999**, *146*, 32.
(13) Young, W. S.; Kuan, W. F.; Epps, T. H. Block Copolymer Electrolytes for Rechargeable Lithium Batteries. *J. Polym. Sci., Part B: Polym. Phys.* **2014**, *52*, 1–16.
(14) Morris, M. A.; An, H.; Lutkenhaus, J. L.; Epps, T. H. Harnessing the Power of Plastics: Nanostructured Polymer Systems in Lithium-Ion Batteries. *ACS Energy Lett.* **2017**, *2*, 1919–1936.
(15) Gopinadhan, M.; Majewski, P. W.; Osuji, C. O. Facile Alignment of Amorphous Poly(Ethylene Oxide) Microdomains in a Liquid Crystalline Block Copolymer Using Magnetic Fields: Toward Ordered Electrolyte Membranes. *Macromolecules* **2010**, *43*, 3286–3293.
(16) Nakamura, I.; Wang, Z. G. Thermodynamics of Salt-Doped Block Copolymers. *ACS Macro Lett.* **2014**, *3*, 708–711.
(17) Marko, J. F.; Rabin, Y. Microphase Separation of Charged Diblock Copolymers: Melts and Solutions. *Macromolecules* **1992**, *25*, 1503–1509.
(18) Sing, C. E.; Zwanikken, J. W.; de la Cruz, M. O. Electrostatic Control of Block Copolymer Morphology. *Nat. Mater.* **2014**, *13*, 694–698.
(19) Kwon, H. K.; Ma, B.; de la Cruz, M. O. Determining the Regimes of Dielectric Mismatch and Ionic Correlation Effects in Ionomer Blends. *Macromolecules* **2019**, *52*, 535–546.
(20) Hou, K. J.; Qin, J. Solvation and Entropic Regimes in Ion-Containing Block Copolymers. *Macromolecules* **2018**, *51*, 7463–7475.
(21) Ganesan, V.; Jayaraman, A. Theory and Simulation Studies of Effective Interactions, Phase Behavior and Morphology in Polymer Nanocomposites. *Soft Matter* **2014**, *10*, 13–38.
(22) Martin, J. M.; Li, W.; Delaney, K. T.; Fredrickson, G. H. Statistical Field Theory Description of Inhomogeneous Polarizable Soft Matter. *J. Chem. Phys.* **2016**, *145*, No. 154104.
(23) Grzetic, D. J.; Delaney, K. T.; Fredrickson, G. H. Field-Theoretic Study of Salt-Induced Order and Disorder in a Polarizable Diblock Copolymer. *ACS Macro Lett.* **2019**, *8*, 962–967.
(24) Nakamura, I.; Wang, Z. G. Salt-Doped Block Copolymers: Ion Distribution, Domain Spacing and Effective χ Parameter. *Soft Matter* **2012**, *8*, 9356–9367.
(25) Teran, A. A.; Balsara, N. P. Thermodynamics of Block Copolymers with and without Salt. *J. Phys. Chem. B* **2014**, *118*, 4–17.
(26) Loo, W. S.; Galluzzo, M. D.; Li, X.; Maslyn, J. A.; Oh, H. J.; Mongcopa, K. I.; Zhu, C.; Wang, A. A.; Wang, X.; Garetz, B. A.; Balsara, N. P. Phase Behavior of Mixtures of Block Copolymers and a Lithium Salt. *J. Phys. Chem. B* **2018**, *122*, 8065–8074.
(27) Chow, T. Miscible Blends and Block Copolymers. Crystallization, Melting, and Interaction. *Macromolecules* **1990**, *23*, 333–337.
(28) Colby, R. H. Breakdown of Time-Temperature Superposition in Miscible Polymer Blends. *Polymer* **1989**, *30*, 1275–1278.
(29) Schmidt, M.; Maurer, F. H. J. Pressure – Volume – Temperature Properties and Free Volume Parameters of PEO/PMMA Blends. *J. Polym. Sci., Part B: Polym. Phys.* **1997**, *36*, 1061–1080.
(30) Lodge, T. P.; Wood, E. R.; Haley, J. C. Two Calorimetric Glass Transitions Do Not Necessarily Indicate Immiscibility: The Case of PEO/PMMA. *J. Polym. Sci., Part B: Polym. Phys.* **2006**, *44*, 756–763.
(31) Silvestre, C.; Cimmino, S.; Martuscelli, E.; Karasz, F. E.; MacKnight, W. J. Poly(Ethylene Oxide)/Poly(Methyl Methacrylate) Blends: Influence of Tacticity of Poly(Methyl Methacrylate) on Blend Structure and Miscibility. *Polymer* **1987**, *28*, 1190–1199.
(32) Eitouni, H. B.; Balsara, N. P. Thermodynamics of Polymer Blends. In *Physical Properties of Polymers Handbook*, 2006; Chapter 19, pp 339–356.
(33) Ito, H.; Russell, T. P.; Wignall, G. D. Interactions in Mixtures of Poly(Ethylene Oxide) and Poly(Methyl Methacrylate). *Macromolecules* **1987**, *20*, 2213–2220.
(34) Matyjaszewski, K. Advanced Materials by Atom Transfer Radical Polymerization. *Adv. Mater.* **2018**, *30*, No. 1706441.

https://dx.doi.org/10.1021/acs.macromol.0c02493
Macromolecules 2021, 54, 1414–1424

(35) Hou, K. J.; Loo, W. S.; Balsara, N. P.; Qin, J. Comparing Experimental Phase Behavior of Ion-Doped Block Copolymers with Theoretical Predictions Based on Selective Ion Solvation. *Macromolecules* **2020**, *53*, 3956−3966.
(36) Wanakule, N. S.; Virgili, J. M.; Teran, A. A.; Wang, Z. G.; Balsara, N. P. Thermodynamic Properties of Block Copolymer Electrolytes Containing Imidazolium and Lithium Salts. *Macromolecules* **2010**, *43*, 8282−8289.
(37) Young, W. S.; Epps, T. H. Salt Doping in PEO-Containing Block Copolymers: Counterion and Concentration Effects. *Macromolecules* **2009**, *42*, 2672−2678.
(38) Mark, J. E. *Physical Properties of Polymers Handbook*, 2nd ed.; Springer: Philadelphia, PA, 2007.
(39) Sun, X.; Zhang, H.; Zhang, L.; Wang, X.; Zhou, Q. F. Synthesis of Amphiphilic Poly(Ethylene Oxide)-b-Poly(Methyl Methacrylate) Diblock Copolymers via Atom Transfer Radical Polymerization Utilizing Halide Exchange Technique. *Polym. J.* **2005**, *37*, 102−108.
(40) Hexemer, A.; Bras, W.; Glossinger, J.; Schaible, E.; Gann, E.; Kirian, R.; MacDowell, A.; Church, M.; Rude, B.; Padmore, H. A SAXS/WAXS/GISAXS Beamline with Multilayer Monochromator A SAXS/WAXS/GISAXS Beamline with Multilayer Monochromator. *J. Phys.: Conf. Ser.* **2010**, *247*, No. 012007.
(41) Ilavsky, J. Nika: Software for Two-Dimensional Data Reduction. *J. Appl. Crystallogr.* **2012**, *45*, 324−328.
(42) Loo, W. S.; Sethi, G. K.; Teran, A. A.; Galluzzo, M. D.; Maslyn, J. A.; Oh, H. J.; Mongcopa, K. I.; Balsara, N. P. Composition Dependence of the Flory−Huggins Interaction Parameters of Block Copolymer Electrolytes and the Isotaksis Point. *Macromolecules* **2019**, *52*, 5590−5601.
(43) Gunkel, I.; Thurn-Albrecht, T. Thermodynamic and Structural Changes in Ion-Containing Symmetric Diblock Copolymers: A Small-Angle X-Ray Scattering Study. *Macromolecules* **2012**, *45*, 283−291.
(44) Naidu, S.; Ahn, H.; Gong, J.; Kim, B.; Ryu, D. Y. Phase Behavior and Ionic Conductivity of Lithium Perchlorate-Doped Polystyrene-b-Poly(2-Vinylpyridine) Copolymer. *Macromolecules* **2011**, *44*, 6085−6093.
(45) Gao, K. W.; Loo, W. S.; Snyder, R. L.; Abel, B. A.; Choo, Y.; Lee, A.; Teixeira, S. C. M.; Garetz, B. A.; Coates, G. W.; Balsara, N. P. Miscible Polyether/Poly(Ether-Acetal) Electrolyte Blends. *Macromolecules* **2020**, *53*, 5728−5739.
(46) Chintapalli, M.; Timachova, K.; Olson, K. R.; Mecham, S. J.; Desimone, J. M.; Balsara, N. P. Lithium Salt Distribution and Thermodynamics in Electrolytes Based on Short Perfluoropolyether-Block-Poly(Ethylene Oxide) Copolymers. *Macromolecules* **2020**, *53*, 1142−1153.
(47) Lin, C. C.; Jonnalagadda, S. V.; Kesani, P. K.; Dai, H. J.; Balsara, N. P. Effect of Molecular Structure on the Thermodynamics of Block Copolymer Melts. *Macromolecules* **1994**, *27*, 7769−7780.
(48) Nakamura, I.; Balsara, N. P.; Wang, Z. G. Thermodynamics of Ion-Containing Polymer Blends and Block Copolymers. *Phys. Rev. Lett.* **2011**, *107*, No. 198301.
(49) Chintapalli, M.; Chen, X. C.; Thelen, J. L.; Teran, A. A.; Wang, X.; Garetz, B. A.; Balsara, N. P. Effect of Grain Size on the Ionic Conductivity of a Block Copolymer Electrolyte. *Macromolecules* **2014**, *47*, 5424−5431.
(50) Huang, J.; Tong, Z. Z.; Zhou, B.; Xu, J. T.; Fan, Z. Q. Salt-Induced Microphase Separation in Poly(ε-Caprolactone)-b- Poly-(Ethylene Oxide) Block Copolymer. *Polymer* **2013**, *54*, 3098−3106.
(51) Gartner, T. E.; Morris, M. A.; Shelton, C. K.; Dura, J. A.; Epps, T. H. Quantifying Lithium Salt and Polymer Density Distributions in Nanostructured Ion-Conducting Block Polymers. *Macromolecules* **2018**, *51*, 1917−1926.
(52) Sethi, G. K.; Jung, H. Y.; Loo, W. S.; Sawhney, S.; Park, M. J.; Balsara, N. P.; Villaluenga, I. Structure and Thermodynamics of Hybrid Organic-Inorganic Diblock Copolymers with Salt. *Macromolecules* **2019**, *52*, 3165−3175.
(53) Borodin, O.; Smith, G. D. Mechanism of Ion Transport in Amorphous Poly(Ethylene Oxide)/LiTFSI from Molecular Dynamics Simulations. *Macromolecules* **2006**, *39*, 1620−1629.
(54) Edman, L. Ion Association and Ion Solvation Effects at the Crystalline-Amorphous Phase Transition in PEO-LiTFSI. *J. Phys. Chem. B* **2000**, *104*, 7254−7258.
(55) Diddens, D.; Heuer, A.; Borodin, O. Understanding the Lithium Transport within a Rouse-Based Model for a PEO/LiTFSI Polymer Electrolyte. *Macromolecules* **2010**, *43*, 2028−2036.

https://dx.doi.org/10.1021/acs.macromol.0c02493
Macromolecules 2021, 54, 1414−1424